# Rayleigh-Bénard Percolation Transition Study of Thermal Convection in Porous Media: Numerical Simulation and NMR Experiments

Markus Weber, Andreas Klemm, and Rainer Kimmich
*Sektion Kernresonanzspektroskopie, Universität Ulm, 89069 Ulm, Germany*
(Received 12 October 2000)

Thermal convection was studied as a function of the porosity in random-site percolation model objects in a Rayleigh-Bénard configuration. NMR velocity mapping experiments and numerical simulations using the finite-volume method are compared. Velocity histograms were evaluated and can be described by power laws in a wide range. The maximum velocity as a function of the porosity indicates a combined percolation/Rayleigh-Bénard transition.

DOI: 10.1103/PhysRevLett.86.4302 PACS numbers: 47.55.Mh, 64.60.Ak

The formation of thermal convection rolls in porous media is strongly obstructed by geometric restrictions. The objective of the present study is to examine the flow velocity distribution in random-site percolation objects as a function of the porosity, $p = V_p/V$, where $V_p$ is the volume of the pore space and $V$ the total volume. Particular attention is to be focused on changes of the flow characteristics in the vicinity of the percolation transition at $p = p_c$.

NMR velocity mapping experiments were carried out in model objects fabricated on the basis of computer-simulated random-site percolation networks. Two spatial and two velocity dimensions were probed with the aid of "Fourier Encoding Velocity Imaging" [1,2].

The experimental data are compared with simulations performed with the finite-volume method (FVM; FLUENT 5.3) [3,4] for the same networks. While thermal convection in free liquids was already studied by different NMR techniques [5,6], there are only a few reports on NMR applications to porous media [7,8].

The templates for the fabrication of the model objects were generated with the aid of a random-number algorithm. The quasi-two-dimensional objects were milled in polystyrene sheets with a circuit board plotter [9,10]. The spatial resolution of the fabrication was 400 $\mu$m, so that all details of the liquid-filled pore space can readily be probed with the spatial resolution of magnetic resonance microscopy. The horizontal and vertical object extension in the network plane was 4 and 2 cm, respectively. The pore space was filled with silicon oil KT5 (TM) with a kinematic viscosity of $\eta = 5 \times 10^{-6}$ m/s$^2$ at 25 °C. There was no perceptible contribution from the solid matrix to the spin echo signals acquired in our experiments. The experimental velocity resolution was 0.01 mm/s.

The attribute "two-dimensional" is to remind us of the base lattice assumed for the generation of the percolation networks. In reality, the objects had a finite width in the third dimension, of course. However, the velocities along this direction were below the noise level ($\approx$0.04 mm/s).

The sample thickness was chosen large enough to ensure a sufficient signal intensity. Thirteen identical, 2 mm thick isolated slabs milled according to the percolation template were glued one on top of the other to form a stack of identical percolation networks with a total fluid layer width of 2.6 cm.

The FVM simulations are based on the Boussinesq approximation [11]. The Navier/Stokes, the continuity, and the heat conduction equations had to be solved with geometrical boundary conditions given by the matrix. The finite thickness of the model objects was not taken into account. The fluid parameters assumed correspond to the silicon oil used in the experiments. Also the heat conductivity of the polystyrene matrix deviating from that of the fluid was accounted for. The convergence criteria of all residuals were $<10^{-5}$. The convergence history of single points was considered as well.

In the experiments, a Rayleigh/Bénard configuration [11,12] was used. Figure 1 shows typical experimental and simulated velocity maps for $\Delta T = 45$ K. In either case the gray levels represent the magnitude of the velocity, $v = \sqrt{v_x^2 + v_y^2}$, where the $y$ axis is along the vertical (temperature gradient) direction. The template generated on a square base lattice with $100 \times 50$ lattice points is also shown for comparison. The symmetric convection patterns typical for the free liquid in the laminar regime (Refs. [5,6] and Fig. 2) are strongly distorted by the matrix obstacles. The experimental and simulated convection patterns correlate well with each other. Some minor deviations at the left and right are attributed to the temperature gradient distributions that are experimentally ill defined near the side walls.

The gray levels in Fig. 1 refer to the magnitude of the velocity relative to the maximum value. The pixel-averaged maximum velocity found in the FVM simulations turned out to be almost four times as large as the maximum NMR value. This is explained by the finite width of the fluid layers in the percolation objects. As a consequence, a Hagen/Poiseuille velocity profile perpendicular to the image plane, i.e., in the third dimension, matters in the real experiments. The mean velocity of such a velocity distribution is just one half of the maximum velocity. On the other hand, the FVM data are based on an ideally two-dimensional transport symmetry. The experimental result

 0031-9007/01/86(19)/4302(4)$15.00 

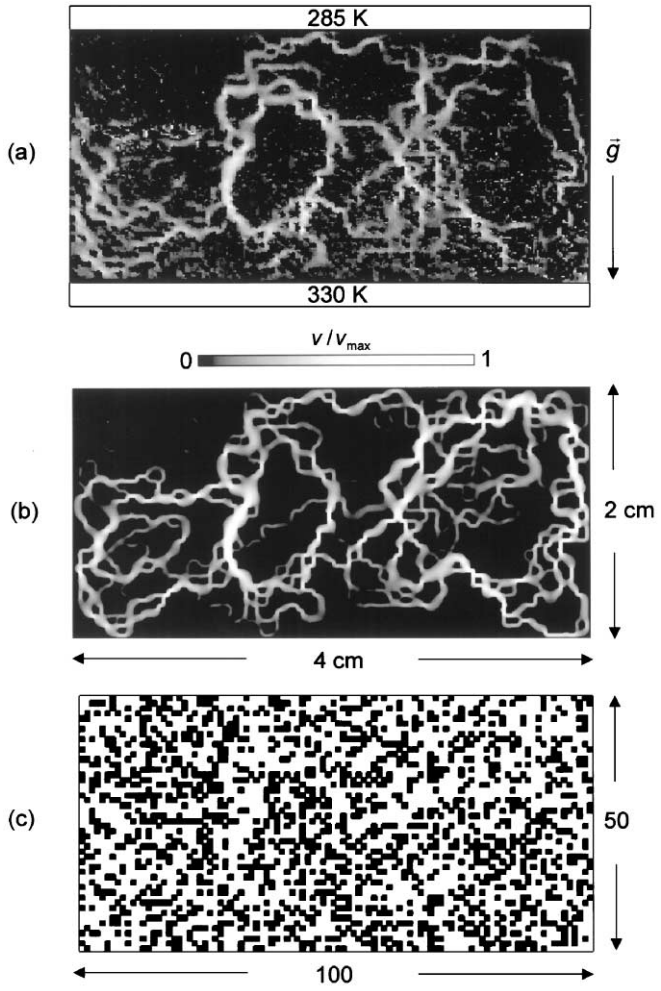


FIG. 1. Velocity maps ($v = \sqrt{v_x^2 + v_y^2}$) of convection patterns in a site-percolation network measured (a) and simulated (b) with NMR velocity mapping and FVM simulation techniques, respectively. The maps refer to a Rayleigh-Bénard configuration with the temperature gradient along the $y$ direction. The NMR experiments were performed in a silicon oil filled model object fabricated on the basis of a computer-generated two-dimensional template (c). The base lattice size is $100 \times 50$, the porosity $p = 0.7 > p_c$. In the simulations, the resolution of each lattice point was $7 \times 7$ elements. The fabrication resolution of the model object is 400 $\mu$m, the experimental digital space resolution 190 $\mu$m. The experimental velocity resolution is 0.01 mm/s. The experimental velocity range probed is $\pm 0.7$ mm/s, the echo and repetition times are 130 and 800 ms, respectively.

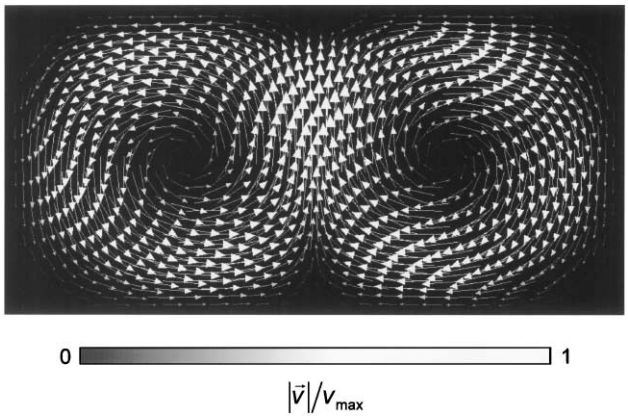


FIG. 2. FVM simulated velocity map ($v = \sqrt{v_x^2 + v_y^2}$) of thermal convection rolls in the bulk for comparison with porous media (see Fig. 1). Prandtl's and Rayleigh's numbers were assumed to be $P_r = 55$ and $R_a = 2345$, respectively. Note that, unlike porous media, convection rolls in the bulk mapped in real experiments tend to be distorted by boundary effects relative to the simulated patterns [6].

may also be slightly affected by partially filled voxels at the matrix edges, whereas full voxels perfectly fitting to the matrix structure are anticipated in the simulations.

In light of the good coincidence of the simulated and experimental flow patterns, we conclude that FVM simulations provide a reliable tool for examining velocity distributions in the submillimeter-per-second range. The advantage of FVM simulations is that the accessible velocity range is much broader than in the NMR experiments which are limited by a finite velocity resolution (here: $\approx 0.01$ mm/s). NMR velocity mapping is therefore feasible only above the Rayleigh-Bénard percolation transition (see below).

The simulated velocity maps visualize the different flow patterns when the geometric restrictions are changed. With decreasing porosity, sample spanning rolls become less likely until a modified percolation transition occurs at a "Rayleigh-Bénard percolation threshold," $p_c^{\mathrm{RB}}$. Note that this transition depends both on the geometric restrictions (as in the ordinary percolation problem) and the hydrodynamic flow properties characteristic for the Rayleigh/Bénard instability.

The critical porosity defined and determined in this way refers to closed loops of the transport pathways in contrast to the ordinary definition that is simply based on the extension of the largest cluster relative to the system. Furthermore, a Rayleigh number modified for porous media may be defined, which effectively accounts for the hydrodynamic properties, the local roll dimensions, and temperature gradients. As a result, one expects $p_c^{\mathrm{RB}}$ to be somewhat *larger* than the ordinary, geometrically defined critical porosity, $p_c$ [13].

Below $p_c^{\mathrm{RB}}$, the convection rolls become more and more localized according to the less extended percolation clusters. Histograms of the velocity magnitude (relative to the respective maximum velocity) are plotted in Figs. 3 and 4 as a function of the porosity. The velocity magnitude was determined at each knot in the meshed area. The total velocity range, $0 \leq v \leq v_{\max}$, was subdivided into 512 or 10 000 equal sections. The abundance of the corresponding knot velocities was then counted and plotted in normalized, double logarithmic form.

The histograms are generally characterized by a flat section at low relative velocities and a sharp drop near the maximum velocities. This finding applies both above and

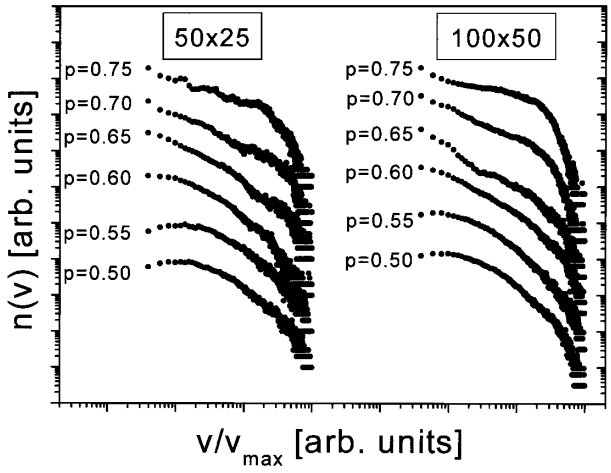


FIG. 3. Velocity histograms evaluated from FVM simulations for 2D random-site percolation networks of different sizes and porosities $p$. The data are plotted versus the ratio of the magnitudes of the local and the maximum velocities, $v/v_{\max}$. The base lattice sizes are $n_x \times n_y = 50 \times 25$ and $100 \times 50$. The $y$ axis represents the vertical direction. The temperature difference is assumed to be $\Delta T = 40$ K (for the Rayleigh-Bénard configuration shown in Fig. 1). The material-specific parameters of silicon oil in a polystyrene matrix were taken into account. The velocity scale was linearly subdivided in 512 intervals. Note that the data points overlap at high velocities owing to the logarithmic scale. The scattering of the data reflects the statistical abundance.

below $p_c^{\mathrm{RB}}$. We attribute the low- and high-velocity regions of the histograms to localized and cluster-spanning convection rolls, respectively. Figure 5 shows a plot of the maximum velocity as a function of the porosity. The Rayleigh-Bénard percolation transition, where a sudden

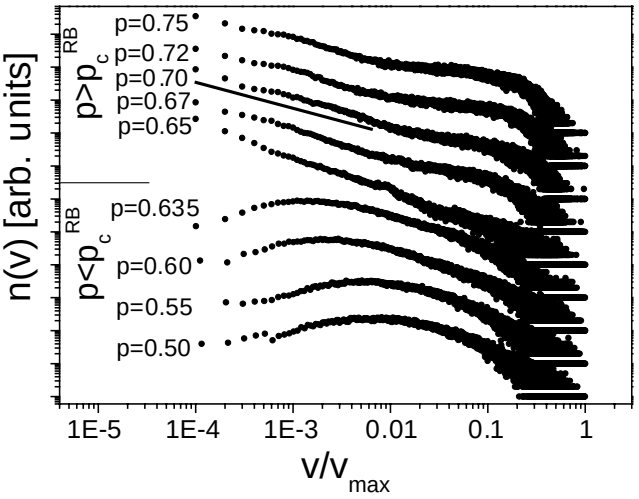


FIG. 4. Velocity histograms analogous to Fig. 3 for a base lattice size is $n_x \times n_y = 100 \times 50$. The velocity scale was linearly subdivided in 10 000 intervals. For $p > p_c^{\mathrm{RB}}$, the data can be described by power laws $n(v) \propto v^{-b}$ with exponents $b = 1.03 \pm 0.1$ ($p = 0.65$); $b = 0.84 \pm 0.1$ ($p = 0.67$); $b = 0.8 \pm 0.1$ ($p = 0.70$; see solid line); $b = 0.72 \pm 0.1$ ($p = 0.72$); $b = 0.71 \pm 0.1$ ($p = 0.75$).

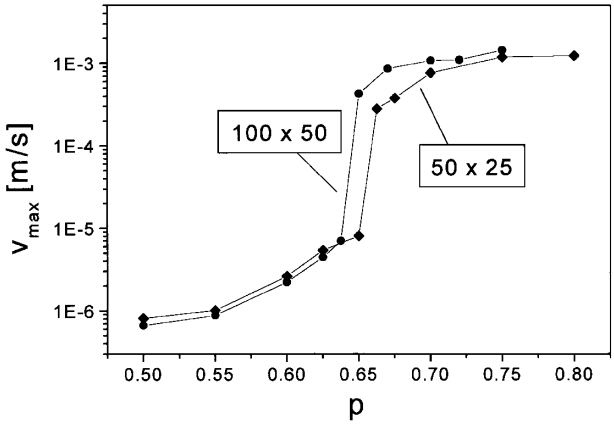


FIG. 5. Magnitude of the maximum velocity as a function of the porosity. The data were evaluated from FVM simulations for two different base lattice sizes $n_x \times n_y$ as in Fig. 3. The solid lines illustrate the Rayleigh-Bénard percolation transitions for the respective system sizes.

change of at least 2 orders of magnitude of the maximum velocity occurs, is obvious.

The ordinary percolation threshold, $p_c$, is predicted to be system size dependent [13]. In the two-dimensional case we have $p_c = p_c^{\infty} + aL^{-3/4}$, where the length $L$ characterizes the extension of the system, $a$ is a constant, and $p_c^{\infty}$ is the value expected for infinite clusters. A similar size dependence appears to be valid for $p_c^{\mathrm{RB}}$ too, where hydrodynamic flow plays a crucial role in addition. Two systems of different base lattice size were investigated. $p_c^{\mathrm{RB}}$ is shifted correspondingly. Note, however, that the temperature difference was kept constant.

Above $p_c^{\mathrm{RB}}$, the distributions of the velocity magnitude of the local convection rolls (that do not span the whole

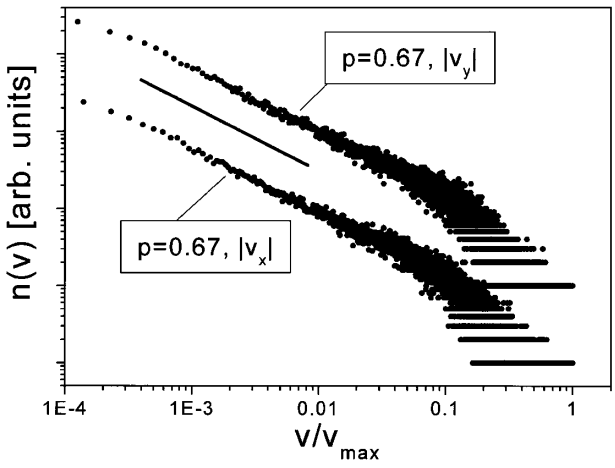


FIG. 6. Histograms of the velocity components $|v_x|$ (horizontal) and $|v_y|$ (vertical) evaluated from FVM simulations. The base lattice size is $100 \times 50$. Analogous to the distribution of the velocity magnitude (Figs. 3 and 4) the data demonstrate the power law behavior in the velocity range of localized convection rolls that do not span the whole cluster, and the velocity cutoff due to cluster-spanning rolls. The solid line corresponds to a power law $n(v) \propto v^{-b}$ with an exponent $b = 0.83 \pm 0.1$.

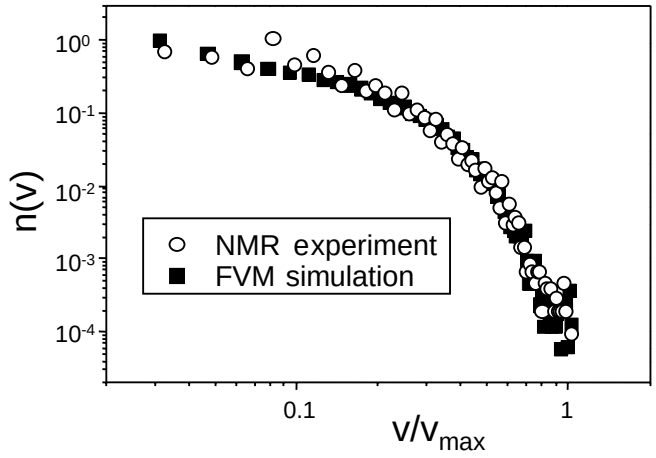


FIG. 7. Normalized velocity histograms evaluated from NMR velocity maps and FVM simulations in the cluster shown in Fig. 1. The velocity scale was linearly subdivided in 64 intervals.

clusters) can be described by power laws, $n(v) \propto v^{-b}$. The same scaling behavior was also found for the velocity components perpendicular ($|v_x|$) and parallel ($|v_y|$) to the temperature gradient (Fig. 6). These power laws describe the data in a wide range below the high-velocity cutoff. The crossover to this cutoff is relatively sharp far above the percolation transition. When approaching and crossing $p_c^{\mathrm{RB}}$ from above, the cutoff region becomes broader and broader. The power law regime may be restricted to such low velocities as $v < v_{\max}/100$. The exponent $b$ depends slightly on the porosity in the sense that higher porosities stipulate a decreasing value of $b$. Interestingly, the results of the present convection study show some features similar to those found in flow studies [14,15].

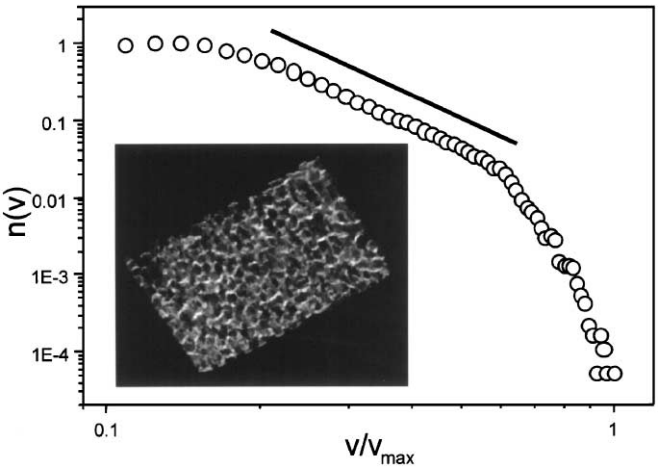


FIG. 8. Normalized histogram of $v = \sqrt{v_x^2 + v_y^2 + v_z^2}$ evaluated from a three-dimensional NMR velocity map of a silicon oil filled polystyrene pellet pack in Rayleigh-Bénard configuration (pellet size 3 to 4 mm, porosity 0.5). The temperature difference was $\Delta T = 75$ K. The velocity scale was linearly subdivided in 64 intervals. The solid line represents a power law $n(v) \propto v^{-b}$ with an exponent $b = 3.05 \pm 0.1$. The inset renders a projection of the three-dimensional experimental velocity map.

NMR velocity mapping is restricted to porosities above $p_c^{\mathrm{RB}}$ for resolution reasons. However, the reliability with which the FVM simulations supplement the experimental data can be quantitatively demonstrated by a direct comparison of experimental and simulated velocity histograms. Figure 7 shows corresponding data evaluated from the velocity maps in Fig. 1.

In order to test the influence of the dimensionality on the experimental velocity distribution, we have also examined an, in the proper sense, three-dimensional system. Figure 8 shows the histogram of $v = \sqrt{v_x^2 + v_y^2 + v_z^2}$ in a silicon oil filled pack of polystyrene pellets. The inset illustrates the flow patterns in the sample. Again a power law was found as expected for $p > p_c^{\mathrm{RB}}$. We conclude that the qualitative behavior is the same as in the quasi-two-dimensional percolation objects, although the slope in the power law regime is much steeper.

[1] T. W. Redpath, D. G. Norris, R. A. Jones, and R. M. S. Hutchinson, Phys. Med. Biol. **29**, 891 (1984).
[2] R. Kimmich, *NMR Tomography, Diffusometry, Relaxometry* (Springer-Verlag, Berlin, 1997).
[3] J. D. Anderson, *Computational Fluid Dynamics* (McGraw-Hill, New York, 1995).
[4] C. Cuvelier, A. Segal, and A. van Steenhoven, *Finite Element Methods and Navier-Stokes Equations* (Reidel, Dordrecht, 1988).
[5] S. J. Gibbs, T. A. Carpenter, and L. D. Hall, J. Magn. Reson. **105**, 209 (1993).
[6] J. Weis, R. Kimmich, and H.-P. Müller, Magn. Reson. Imaging **14**, 319 (1996).
[7] M. D. Shattuck, R. P. Behringer, G. A. Johnson, and J. G. Georgiadis, Phys. Rev. Lett. **75**, 1934 (1995).
[8] L. Howle, R. P. Behringer, and J. Georgiadis, Nature (London) **362**, 230 (1993).
[9] H.-P. Müller, J. Weis, and R. Kimmich, Phys. Rev. E **52**, 5195 (1995).
[10] A. Klemm, H.-P. Müller, and R. Kimmich, Phys. Rev. E **55**, 4413 (1997).
[11] D. J. Tritton, *Physical Fluid Dynamics* (Oxford Science Publications, Oxford, 1988).
[12] D. A. Nield and A. Bejan, *Convection in Porous Media* (Springer-Verlag, Berlin, 1992).
[13] D. Stauffer and A. Aharony, *Introduction to Percolation Theory* (Taylor and Francis, London, 1992).
[14] J. S. Andrade, Jr., M. P. Almeida, J. Mendes Filho, S. Havlin, B. Suki, and H. E. Stanley, Phys. Rev. Lett. **79**, 3901 (1997).
[15] H. A. Makse, J. S. Andrade, Jr., and H. E. Stanley, Phys. Rev. E **61**, 583 (2000).